RSC Advances

PAPER

View Article Online
View Journal | View Issue

Cite this: *RSC Adv.*, 2023, **13**, 25069

High quantum efficiency and excellent color purity of red-emitting Eu^{3+}-heavily doped $Gd(BO_2)_3$-Y_3BO_6-$GdBO_3$ phosphors for NUV-pumped WLED applications

Manh Trung Tran,[a] Nguyen Van Quang,[b] Nguyen Thi Huyen,[b] Nguyen Tu,*[c] Nguyen Van Du,[c] Do Quang Trung,[c] Nguyen Tri Tuan,[d] Nguyen Duy Hung,[e] Dao Xuan Viet,[e] Duong Thanh Tung,[e] Nguyen Duc Trung Kien,[f] Tong Thi Hao Tam[g] and Pham Thanh Huy[a]

Eu^{3+}-doped phosphors have been much attractive owing to their narrow-band red emission peak at 610–630 nm with high color purity; however, the weak and narrow absorption band in the NUV region limits their applications. Doping a higher amount of Eu^{3+} ions into a non-concentration quenching host could be key to enhancing the efficiency of the absorption value and emission intensity. Hence, the design of Eu^{3+}-heavily doped phosphors with a suitable host lattice is key for applications. In this study, red-emitting Eu^{3+}-doped $Gd(BO_2)_3$-Y_3BO_6-$GdBO_3$ (GdYGd:Eu^{3+}) phosphor with a high quantum efficiency of 58.4% and excellent color purity of 99.5% is reported for the first time. The phosphor is efficiently excited by NUV light at 394 nm and emits a strong red emission band in the 590–710 nm range, peaking at 612 nm. The optimal annealing temperature and Eu^{3+} doping content to obtain the strongest PL intensity are 1100 °C and 20 mol%, respectively. The optimized GdYGd:Eu^{3+} phosphor possesses a high activation energy of 0.319 eV and a lifetime of 1.14 ms. An illustration of phosphor-coated NUV LED with chromaticity coordinates ($x = 0.5636, y = 0.2961$) was successfully synthesized, demonstrating the great potential of GdYGd:Eu^{3+} phosphor for NUV-pumped WLED applications.

Received 13th June 2023
Accepted 7th August 2023

DOI: 10.1039/d3ra03955b

rsc.li/rsc-advances

1. Introduction

Phosphor-converted white light-emitting diodes (pc-WLEDs) are widely used in industry and life because of their many advantages, such as a long lifetime, less thermal radiation, high efficiency, low energy consumption, and eco-friendliness.[1] Pc-WLEDs are typically fabricated by combining LED chips with down-converting phosphors.[2] Commercially available WLEDs are often obtained by placing the yellow-emitting YAG:Ce^{3+} phosphor on a blue LED chip (InGaN-460 nm).[3] However, this approach has some drawbacks, such as a poor color rendering index (CRI < 80) and highly unexpected correlated color temperature (>4000 K) due to the shortage of red emission.[4] Consequently, significant efforts have been dedicated to exploring viable solutions to manipulate white light through the relevant combination of red, green, and blue (RGB) emissions.[5] The most common high-CRI pc-WLED is produced by two main techniques: (i) covering green and red-emitting phosphors on a blue LED chip and (ii) coating a mixture of blue, green, and red-emitting phosphors on a near-UV (NUV) LED chip.[6] Over the past few decades, enormous RGB phosphors have been discovered; however, the efficiency of red-emitting phosphors has not satisfied the need for practical application in low brightness.[1] This obstacle has become more severe for red-emitting phosphors because of the low sensitivity of human eyes to the red and far-red spectral region.[7] According to the literature, europium (Eu^{2+} and Eu^{3+}) and manganese (Mn^{4+}) ions are prevalently used as activators for red-emitting phosphors.[8] The most favorable selection for commercial applications is Eu^{2+}-doped phosphors owing to their broad absorption band in the range of 400–480 nm is well matched with the blue LED chip emission.[9] Unfortunately, the synthesis of these phosphors requires very harsh conditions, such as extreme

[a]*Faculty of Materials Science and Engineering, Phenikaa University, Yen Nghia, Ha-Dong district, Hanoi 10000, Vietnam*
[b]*Department of Chemistry, Hanoi Pedagogical University 2, Phuc Yen, Vinh Phuc, Vietnam*
[c]*Faculty of Fundamental Sciences, Phenikaa University, Yen Nghia, Ha-Dong district, Hanoi 10000, Vietnam. E-mail: tu.nguyen@phenikaa-uni.edu.vn*
[d]*College of Science, Cantho University, 3/2 Ninh Kieu, Cantho 94000, Vietnam*
[e]*International Training Institute for Materials Science (ITIMS), Hanoi University of Science and Technology (HUST), 01 Dai Co Viet, Hanoi, 10000, Vietnam*
[f]*Faculty of Electrical and Electronic Engineering, Phenikaa University, Yen Nghia, Ha-Dong district, Hanoi 10000, Vietnam*
[g]*School of Information Technology and Digital Economics (SITDE), National Economics University (NEU), 207 Giai Phong Street, Hanoi 10000, Vietnam*

temperature (1800 °C), excessive atmosphere (0.9 MPa), and an inert gas (N_2), leading to high cost.[10] In addition, the use of blue excitation causes significant reabsorption and reduces the quality of output light.[11] Eu^{3+}-doped phosphors could solve this issue because of the featured excitation in the NUV region (360–420 nm).[5] Owing to the characteristic $^5D_0 \rightarrow {}^7F_J$ ($J = 1, 2, 3$, and 4) transitions, Eu^{3+}-doped phosphors could produce narrow-band orange-red/red emissions, in which the orange-red (610–630 nm) emission, corresponding to the $^5D_0 \rightarrow {}^7F_2$ transition, is appropriate for indoor or full-color display applications with high color purity.[8] However, NUV-pumped pc-WLED using the Eu^{3+}-doped phosphors show a low quantum efficiency (QE) owing to the negligible absorption in the NUV and blue region, resulting from the parity-forbidden transitions ($^7F_0 \rightarrow {}^5D_4$, $^5L_6$, $^5D_3$).[12] It is well known that red-emitting $Y_2O_2S:Eu^{3+}$, green-emitting ZnS:Cu^+, Al^{3+}, and blue-emitting $BaMgAl_{10}O_{17}:Eu^{2+}$ phosphors are currently used for UV InGaN-based WLED; however, the efficiency of green and blue phosphors is eight times higher than that of red phosphor.[13] In addition, the life duration of $Y_2O_2S:Eu^{3+}$ material is insufficient under prolonged UV irradiation.[6] Thus, NUV-pumped novel red-emitting phosphors with high efficiency are in great demand to replace the current $Y_2O_2S:Eu^{3+}$ material for emerging applications.[4]

On the one hand, higher efficiency of absorption value and emission intensity could be achieved by doping more Eu^{3+} dopant content in non-concentration quenching hosts, such as $Ca_3Y_{2-x}B_4O_{12}:xEu^{3+}$ (ref. 14) or $Ba_6Gd_{2(1-x)}Ti_4O_{17}:xEu^{3+}$.[5] On the other hand, developing a suitable host matrix for NUV-excited WLED is also considered to provide non-inversion symmetry sites for dopant Eu^{3+} ions.[15] Accordingly, high-brightness red-emitting Eu^{3+}-doped phosphors well excited at 395 nm, such as $Ca_3(PO_4)_2:Eu^{3+}$ (ref. 16) and $Sr_3Y(BO_3)_3:Eu^{3+}$,[3] are interesting for use in NUV-pumped LEDs. Another prominent candidate, the $AlPO_4:Eu^{3+}$ phosphor, with high quantum efficiency and excellent thermal stability for NUV-pumped WLED, has been reported in our previous study.[8] It was previously reported that $GdBO_3$,[17–19] $Gd(BO_2)_3$,[20] and Y_3BO_6 (ref. 21 and 22) are excellent host lattices to dope a high amount of Eu^{3+} ions; however, only a low quantum efficiency of 14.30% could be obtained under the excitation of NUV light. It is well known that the introduction of dopants at a critical concentration in a material often leads to a decrease in photoluminescence (PL) intensity, resulting in a lower quantum efficiency of the synthesized material.[8] To enhance quantum efficiency, one effective approach is the heavy doping of the host lattice.[23,24] Significantly, this can be accomplished within multi-phase lattices, offering a compelling pathway for optimizing the optical properties of the material.[25]

Herein, a novel Eu^{3+}-heavily doped $Gd(BO_2)_3$-Y_3BO_6-$GdBO_3$ (GdYGd:Eu^{3+}) NUV-pumped red-emitting phosphors with high quantum efficiency and excellent color purity. The influence of synthesis parameters on the crystal structure and luminescence characteristics has been systematically studied. Further, the chromaticity coordinates, color purity, thermal stability, and quantum efficiency of synthesized phosphors are discussed. A prototype of a phosphor-converted NUV LED is fabricated, demonstrating the high potential for NUV-pumped WLED applications.

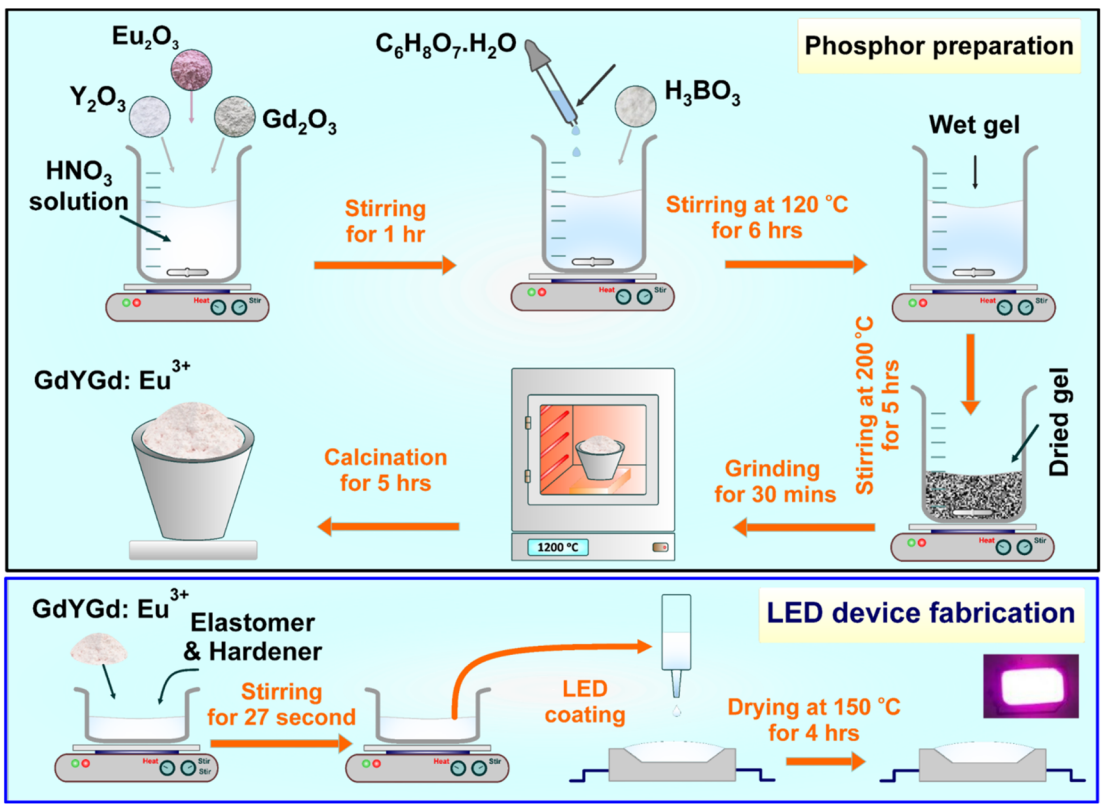

Fig. 1 Schematic fabrication procedure for the Eu^{3+}-doped $Gd(BO_2)_3$-Y_3BO_6-$GdBO_3$ phosphors and LED device.

2. Materials and methods

2.1. Material preparation

The red-emitting GdYGd:Eu^{3+} phosphor was obtained by applying a simple sol–gel method using the initial materials, including Y_2O_3 (Sigma-Aldrich 99.99%), Eu_2O_3 (Sigma-Aldrich 99.99%), Gd_2O_3 (Sigma-Aldrich 99.99%), H_3BO_3 (Sigma-Aldrich 99.99%), $C_6H_8O_7 \cdot H_2O$ (Sigma-Aldrich 99.99%) and HNO_3 (Merck, 67%). First, Y_2O_3, Eu_2O_3, and Gd_2O_3 oxides were magnetically stirred at room temperature in an HNO_3 solution for 60 minutes to dissolve completely. During this process, H_3BO_3 and $C_6H_8O_7 \cdot H_2O$ solutions were gradually dropped to obtain a transparent solution. Then, this solution was continuously stirred at 120 °C for 6 h to obtain a wet gel product. The wet gel was also stirred at 200 °C for 5 h to obtain a dry gel. The dry gel was ground using an agate mortar for 30 minutes in the next step. Finally, the received product was annealed at 600–1200 °C in the air for 5 h to achieve the final GdYGd:Eu^{3+} phosphor powders.

2.2. LED device fabrication

A red LED was produced using the following procedure. First, an elastomer and a hardener were mixed in a proportion of 1 : 1 to obtain a polydimethylsiloxane solution (PDMS, Dow Corning OE-7340 Optical Encapsulant). Then, the optimized GdYGd:Eu^{3+} phosphor was incorporated with a PDMS solution

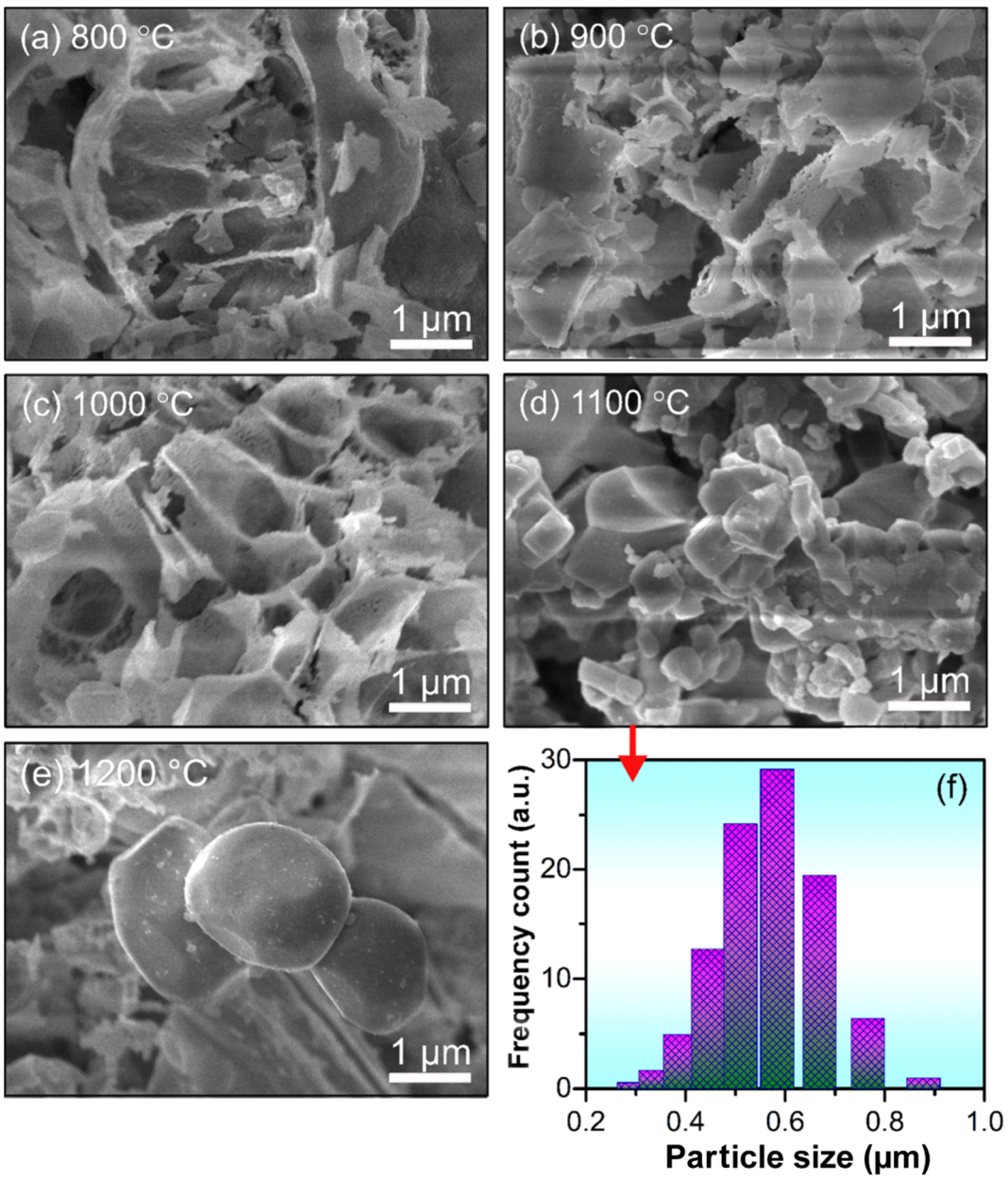

Fig. 2 (a–e) FESEM images of GdYGd:20 mol% Eu^{3+} phosphor annealed at different temperatures in the range of 800–1200 °C for 5 h and (f) grain-size distribution of GdYGd:20 mol% Eu^{3+} phosphor annealed at 1100 °C for 5 h.

(phosphor : PDMS = 1 : 4) by applying a 27-second process utilizing a planetary mixer (Kurabo Mazerustar KK-V300SS). The red LED prototype was obtained by putting the prepared mixture on the cover of a NUV 395 nm chip utilizing a dispenser (i-DR S310A Desktop Dispensing Systems), followed by a 4 h dried process at 150 °C using an oven (ASONE AVO-310SB-D). The schematic fabrication procedure for GdYGd:Eu^{3+} phosphors and LED device are presented in Fig. 1.

2.3. Characterization

The crystalline structure of all samples was characterized by a D8 Advance X-ray diffractometer using CuKα (λ_{Cu} = 1.5406 Å) radiation. The surface morphology of the samples was investigated by field emission scanning electron microscopy (FESEM-JEOL/JSM-7600F). The grain size variation was evaluated using an LB-550 dynamic light scattering system (Horiba, USA). Photoluminescence (PL, 3D PL) and photoluminescence excitation (PLE) spectra were studied using a NanoLog fluorescence spectrophotometer (Horiba, USA) with a 450 W xenon lamp. The optical characterization of the red LED illustration was investigated with a GS-1290-3 spectroradiometer (Gamma Scientific, USA) using an integrating sphere with a diameter of 50 cm. All the above characterizations were carried out under ambient conditions.

3. Results and discussion

3.1. Surface morphology and structure analysis

Fig. 2a–e shows the FESEM images of GdYGd:20 mol% Eu^{3+} phosphor annealed at different temperatures in the range of 800–1200 °C for 5 h. It was observed that the particle size of the samples tended to increase gradually with an increase in annealing temperature. This could be explained by the agglomeration of small clusters forming larger particles at high temperatures.[26] As shown in Fig. 2d and f, the FESEM image and the size variation of GdYGd:20 mol% Eu^{3+} phosphor annealed at 1100 °C confirmed that the average size of particles is about 0.6 μm. The largest particle size of 2 μm is obtained at 1200 °C.

Fig. 3 shows the XRD patterns of GdYGd:20 mol% Eu^{3+} phosphors annealed in the air for 5 h at 600–1200 °C. Only low-

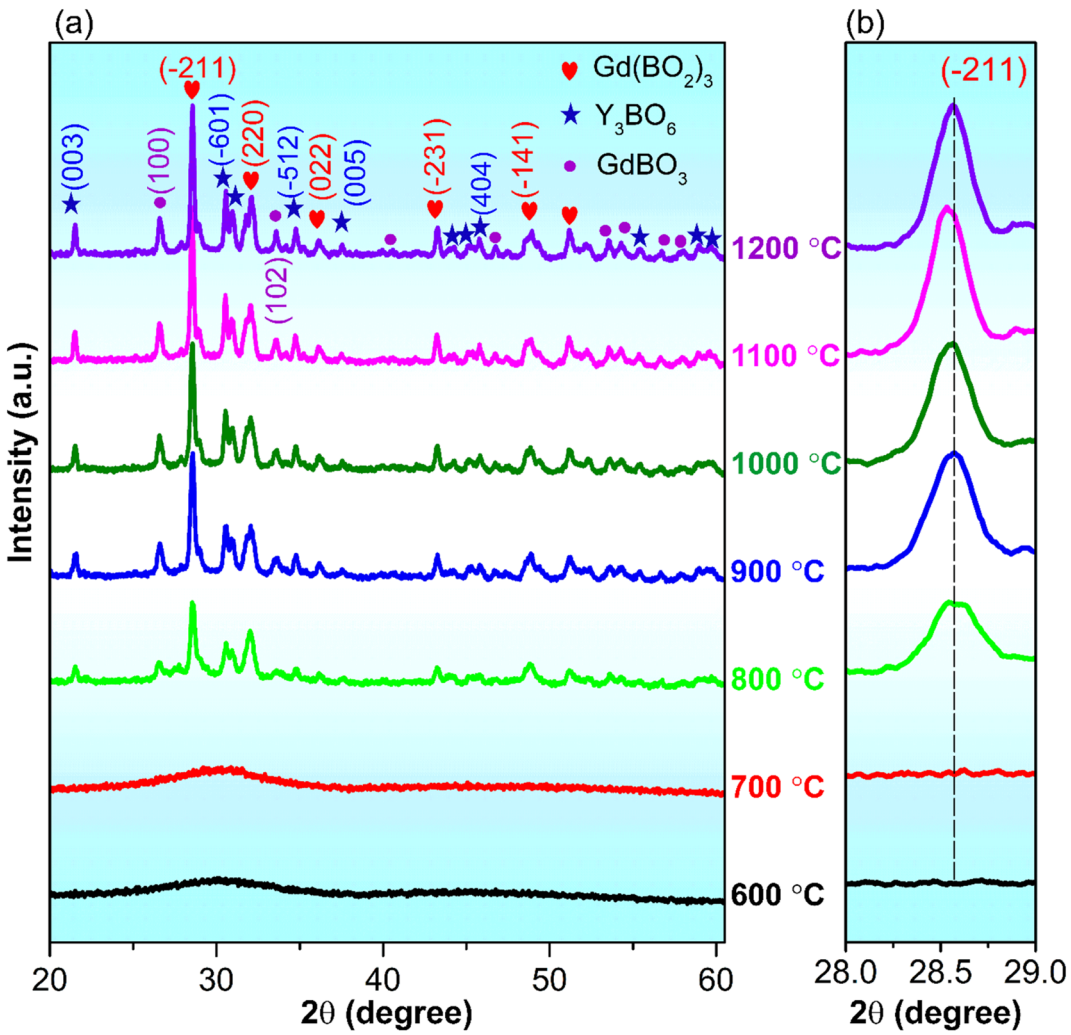

Fig. 3 (a) XRD patterns of GdYGd:20 mol% Eu^{3+} phosphors annealed in air at the temperature range of 600–1200 °C for 5 h and (b) in-focused XRD pattern of the (−211) plane.

intensity diffraction peaks could be observed in the XRD patterns of samples annealed at low temperatures of 600–700 °C, indicating a low crystalline quality of obtained samples. At 800 °C, multiple sharp peaks are obtained at $2\theta = 21.5°$, 26.5°, 28.5°, 30.4°, 31.9°, 33.5°, 34.4°, 36.2°, 43.2°, 45.8°, 48.7°, 51.2°, and 54.2°, corresponding to the coexistence of three different phases, including monoclinic $Gd(BO_2)_3$ (JCPDS no. 23-0986),[27] monoclinic Y_3BO_6 (JCPDS no. 34-0291)[6] and hexagonal $GdBO_3$ structures (JCPDS no. 13-0483).[28] It is noteworthy that the peak intensity generally increases with an increase in the temperature from 800 to 1100 °C and then slightly decreases at 1200 °C, implying that $Gd(BO_2)_3$, Y_3BO_6, and $GdBO_3$ phases started forming at 800 °C and reached the best crystalline quality at 1100 °C. It should also be noted that there is a modest shift toward lower angles with an increase in temperature from 800 to 1100 °C, probably relating to the substitution of the larger-radius ion (Eu^{3+}: 0.95 Å) for the smaller one (Y^{3+}: 0.88 Å) in the host lattice.[29,30] The shift towards a higher angle at 1200 °C could possibly be related to the replacement of larger-sized Gd^{3+} ions (1.25 Å)[27] by smaller-radius-size Eu^{3+} ions.[3,16]

Fig. 4a and b illustrate the XRD patterns and in-focused XRD pattern at the (−211) plane of GdYGd:x mol% Eu^{3+} (x = 1–35) phosphors annealed at 1100 °C for 5 h, respectively. As shown in Fig. 4a, all XRD patterns exhibit a similar shape, indicating a slight influence of Eu^{3+} ion concentration on the crystalline structure of GdYGd:Eu^{3+} phosphors. Fig. 4b reveals a fluctuation of peak position at the dopant level of 1–23 mol% and a shift towards a larger 2θ angle with a further increase in Eu^{3+} ion concentration. Although Eu^{3+} ions could replace Y^{3+} or/and Gd^{3+} ions in the host lattice,[3,6,11] they are preferentially substituted by Y^{3+} ions owing to a slight difference in radius between Eu^{3+} and Y^{3+} ions.[29,30] Hence, the negligible variation in the (−211) peak at Eu^{3+} doping concentrations of 1–23 mol% could be explained well by substituting Eu^{3+} with Y^{3+} ions. In contrast, the right shift at the higher Eu^{3+} doping content (>23 mol%) implies the dominance of the substitution of Eu^{3+} ions for Gd^{3+} ions when the saturated replacement of Eu^{3+} for Y^{3+} ions is reached in the host lattice.[11,31]

3.2. Photoluminescence study

Fig. 5a presents the PLE and PL spectra of GdYGd:20 mol% Eu^{3+} phosphor annealed at 1100 °C for 5 h. The PLE spectrum monitored at 612 nm shows a strong broad absorption band

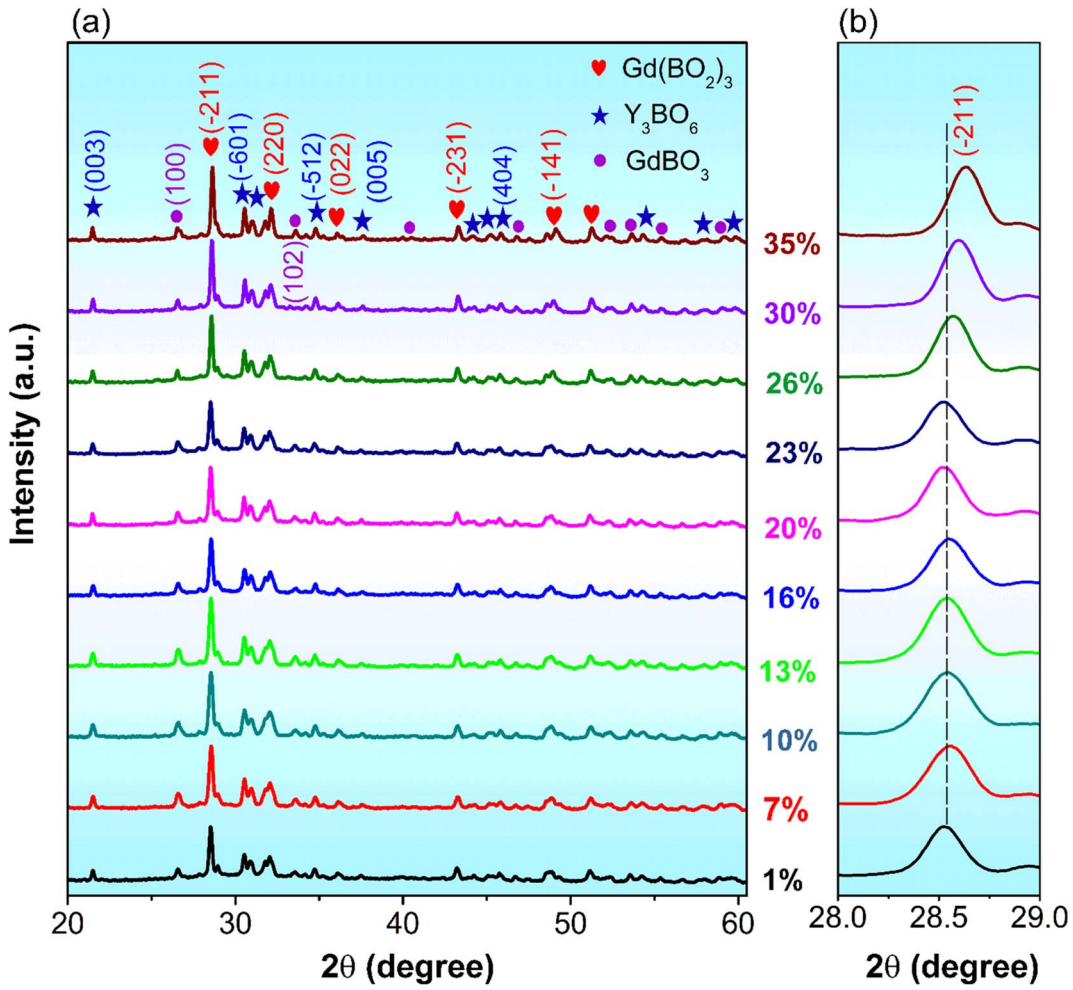

Fig. 4 (a) XRD patterns of $Gd(BO_2)_3$-Y_3BO_6-$GdBO_3$:x mol% Eu^{3+} (x = 1–35) phosphors annealed at 1100 °C for 5 h and (b) in-focused XRD pattern of the (−211) plane.

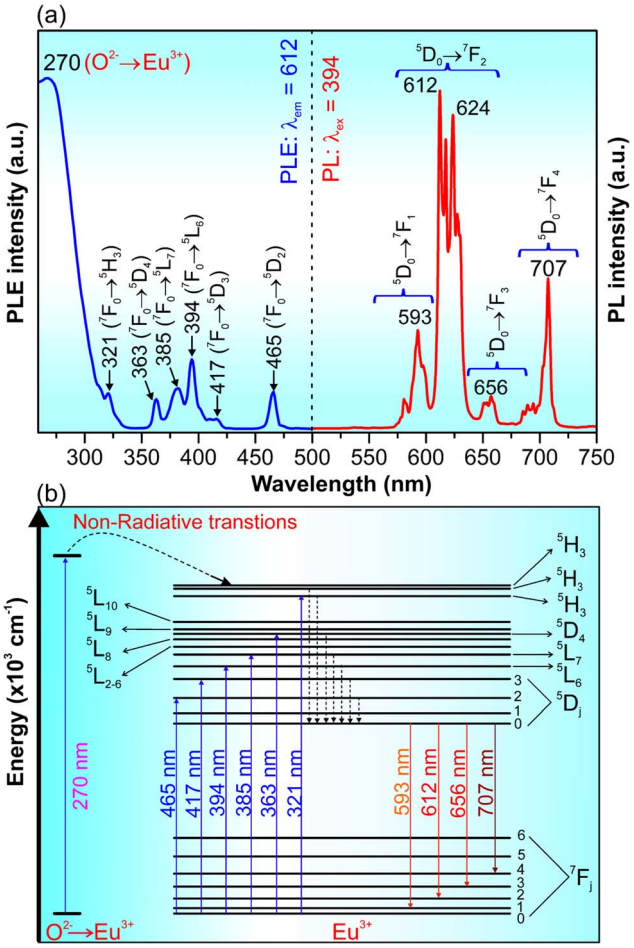

Fig. 5 (a) PLE spectrum (blue curve) monitored at 612 nm and PL spectrum (red curve) excited at 394 nm of GdYGd:20 mol% Eu^{3+} phosphors annealed in air at 1100 °C for 5 h. (b) A diagram of the energy level for excitation and emission transition of Eu^{3+} in $Gd(BO_2)_3$-Y_3BO_6-$GdBO_3$ host lattice.

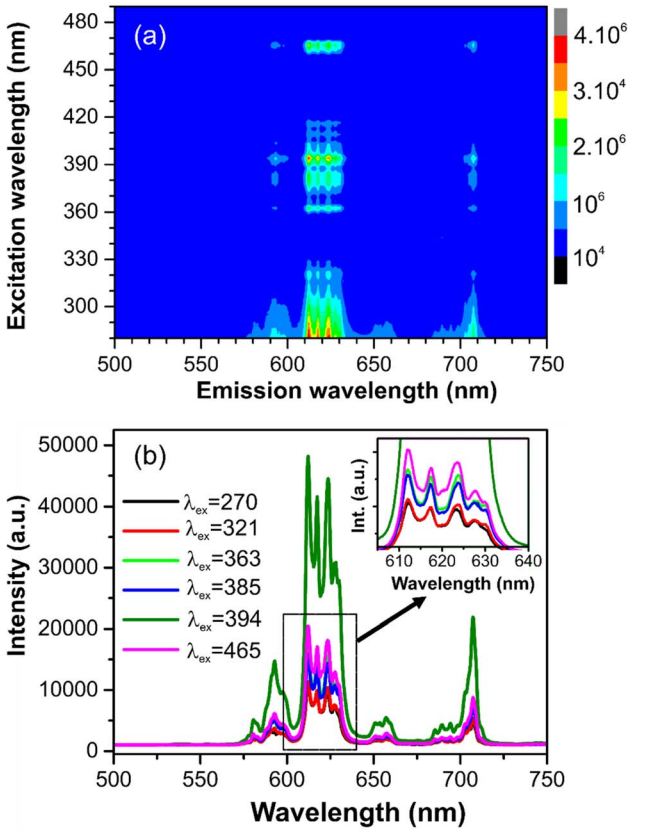

Fig. 6 (a) 3D emission–excitation spectrum and (b) PL spectra excited at 270, 321, 363, 385, 394, and 465 nm of the GdYGd:20 mol% Eu^{3+} phosphors annealed in the air at 1100 °C for 5 h.

peaking at 270 nm and lower-intensity peaks at 321, 363, 385, 394, 417 and 465 nm. It has been previously reported that the strong and broad peak at around 270 nm is due to the Eu^{3+}–O^{2+} transition in the host lattice.[8] The peaks at 321, 363, 385, 394, 417 and 465 nm correspond to the $^7F_0 \rightarrow {}^5H_3$, $^7F_0 \rightarrow {}^5D_4$, $^7F_0 \rightarrow {}^5L_7$, $^7F_0 \rightarrow {}^5L_6$, $^7F_0 \rightarrow {}^5D_3$ and $^7F_0 \rightarrow {}^5D_2$ transitions of Eu^{3+} ions,[32–37] respectively. The PL spectrum excited at 394 nm shows multiple emissions in the red-light region at 593, 612, 617, 624, 627, 656, and 707 nm, attributing to the $^5D_0$–^7F_j ($j = 1, 2, 3, 4$) transitions of Eu^{3+} ions.[6,34,38–47] Briefly, the peak at 593 nm is due to the $^5D_0$–$^7F_1$ transition; the emission peaks at 612–627 nm and 656 nm originated from the $^5D_0$–$^7F_2$ and $^5D_0$–$^7F_3$ transitions, respectively. The peak at 707 nm is due to the $^5D_0$–$^7F_4$ transition of Eu^{3+} ions. A diagram of the energy levels for the excitation and emission transitions of Eu^{3+} ions in GdYGd lattices is illustrated in Fig. 5b.

The 3D emission and excitation spectrum and PL spectra under the excitation of different wavelengths of GdYGd:20 mol% Eu^{3+} phosphors annealed at 1100 °C for 5 h are illustrated in Fig. 6a and b, respectively. The 3D emission and excitation spectrum in Fig. 6a demonstrate that the as-synthesized phosphor has three absorption regions at (i) 280–330 nm; (ii) 355–425 nm with the highest intensity peak at 394 nm; and (iii) 450–470 nm with the most substantial peak at 465 nm. As shown in Fig. 6b, the intensity of the PL spectrum excited at 394 nm is the highest compared to the PL spectra excited at 270, 321, 363, 385, and 465 nm, which confirms the most suitable excitation wavelength at 394 nm. Several other emissions could also be observed in the red-light region, in the range of 590–710 nm.

Fig. 7 displays the PL spectra of GdYGd:20 mol% Eu^{3+} phosphors annealed at 700–1200 °C for 5 h. While no emission could be observed at 700 °C, multiple emission peaks are observed in the PL spectra of the phosphors annealed at 800–1200 °C. This observation is well explained by the better crystalline structure of the higher-temperature-annealed phosphors, as shown in Fig. 3. It is also noted that all PL spectra of samples annealed at 800–1200 °C show an indistinguishable shape; however, there is a strong relationship between the PL intensity and the synthesized temperature. As illustrated in the inset of Fig. 7, the 612 nm peak intensity first increases with the temperature in the range of 800–1100 °C, reaching the highest value at 1100 °C, and then decreases with the higher temperature of 1200 °C. The improvement in the PL intensity at 800–1100 °C could be associated with more efficient diffusion of Eu^{3+} ions into the GdYGd host lattice or/and a significant

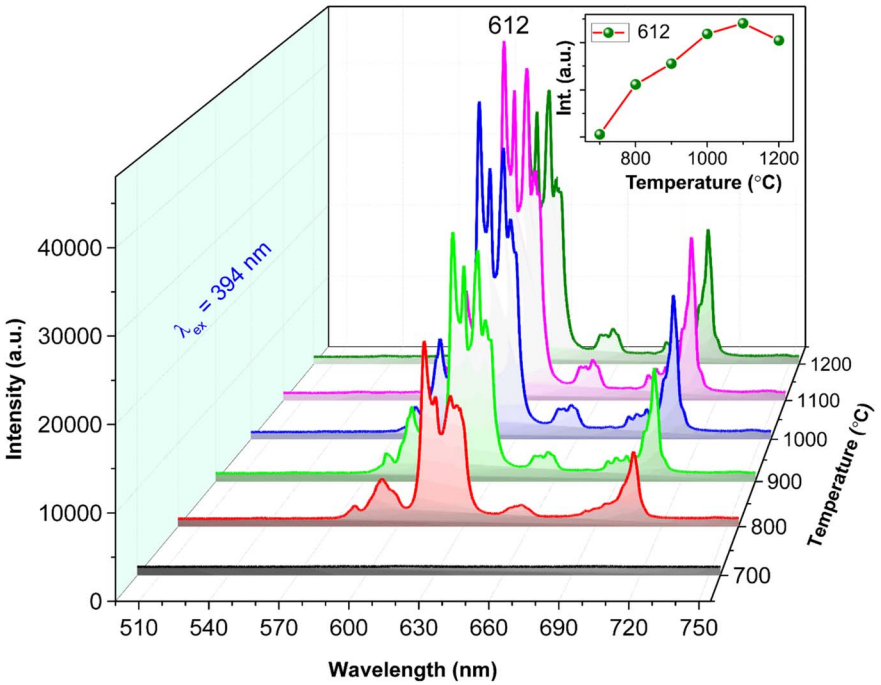

Fig. 7 PL spectra excited by the 394 nm wavelength of GdYGd:20 mol% Eu^{3+} phosphors annealed in the air at 600–1200 °C for 5 h.

improvement in the quality of GdYGd crystalline phases at elevated temperatures.[8] The lower PL intensity at 1200 °C could be explained by the reduction in the crystalline quality of the GdYGd phases, as previously shown in the XRD patterns.

Fig. 8 illustrates the PL spectra of GdYGd:x mol% Eu^{3+} (x = 1–35%) phosphors synthesized at 1100 °C in air for 5 h, showing a significant influence of Eu^{3+} dopant concentrations on the PL intensity. The inset of Fig. 8 establishes the change in the 612

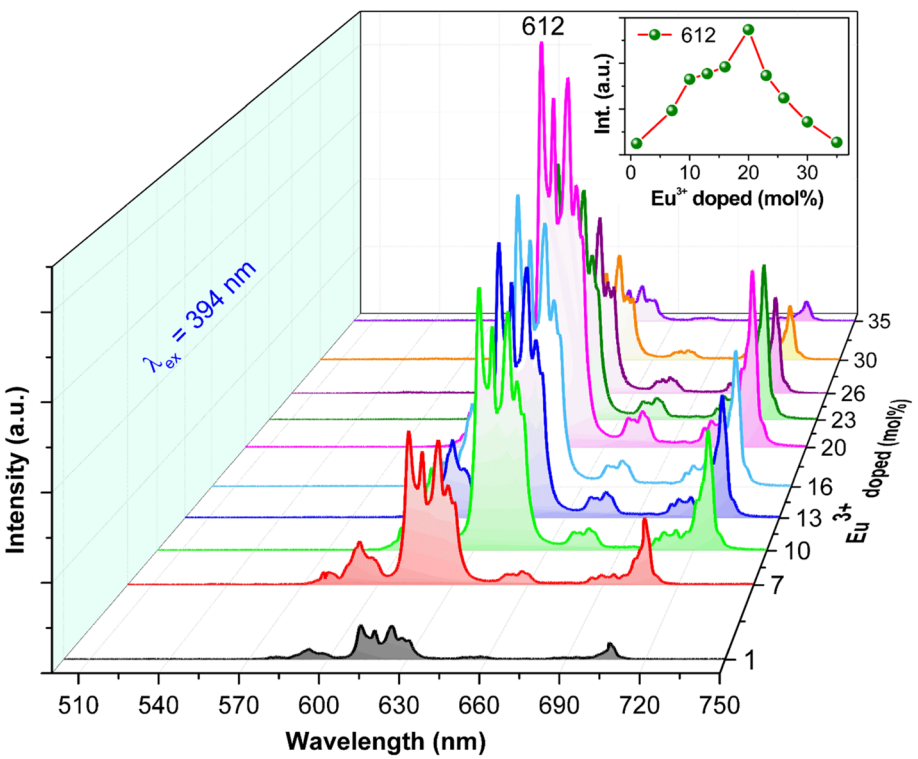

Fig. 8 PL spectra excited at 394 nm of GdYGd:x mol% Eu^{3+} (x = 1–35) phosphors annealed at 1100 °C for 5 h. The inset shows the 612 nm peak intensity dependence on Eu^{3+} concentrations.

nm peak intensity with the Eu^{3+} doping concentration. It is evident that the PL intensity gradually increases with the dopant Eu^{3+} concentration in the range of 1–20 mol%, which is explained by an increase in the luminescent centers.[8] Then, it decreases with higher concentrations from 20 to 35 mol% Eu^{3+}, possibly relating to the quenching effect of concentration.[48] The most intense PL intensity is obtained at 20 mol%, indicating that the distance between neighbor Eu^{3+} ions reached its critical distance threshold, R_c.[8,11,48] In this case, the R_c value of 7.02 Å can be determined using the Blasse equation, which is higher than the critical value of 5 Å for exchanging energy by interaction, implying the governance of the multipolar interaction for the quenching mechanism.[8,16] It is well known that multipolar interaction often contains three types that correspond to the value of the characteristic function for multipolar interaction types: dipole–dipole, dipole–quadrupole, and quadrupole–quadrupole interactions.[49] In this study, the dipole–quadrupole interaction majorly governs the multipolar interaction of Eu^{3+} ions in the GdYGd host lattice. Similar results have also been reported in our previous study.[8]

Fig. 9a and b show the PLE spectra monitored at 612 nm and the time-resolved decay spectra using the excitation wavelength of 394 nm for GdYGd:x mol% Eu^{3+} (x = 7–30) samples, respectively. Although all the PLE spectra shown in Fig. 9a present a unique shape with three main absorption regions at 260–330 nm, 355–425 nm, and 450–470 nm, the PLE intensity strongly depends on the doping concentrations. It first increases as the dopant concentrations increase from 7 to 20 mol% and then decreases with higher concentrations of 23 and 30 mol%. The highest PLE intensity is reached at 20 mol%, as demonstrated in the inset of Fig. 9a. As described in our previous study, PL decay curves can be fitted using a double-exponential function.[50] As shown in Fig. 9b, the fitted lifetime values of Eu^{3+}-doped GdYGd phosphors are in the order of milliseconds, which is consistent with the values reported in recent studies.[51,52] It is noteworthy that there is a slight decrease in the lifetime from 1.18 to 1.12 ms with an increase in Eu^{3+} doping concentration from 7 to 30 mol%, highly contributing to the quenching effect by concentration.[51] This means that the highest PL intensity could be obtained at a doping concentration of 20 mol%.

3.3. Color purity, thermal stability, and quantum efficiency (QE)

It is well known that the chromaticity coordinates (x,y), color purity, and thermal stability of phosphors are important factors for LED applications.[11] The calculated (x,y) values of all the samples are displayed in Fig. 10, beyond the red-light region of the CIE diagram. In addition, the color purity can be calculated from the CIE coordinates.[53] Table 1 presents the (x,y) values of all the samples under an excitation wavelength of 394 nm. It is noteworthy that the GdYGd:x mol% Eu^{3+} (x = 1–35) phosphors possess excellent color purities (higher than 99% at all the Eu^{3+} doping concentrations), which is superior to those of $K_2SrGe_8O_{18}$: Eu^{3+} (95.5%),[54] $Na_2Gd(PO_4)(MoO_4)$:Eu^{3+} (92%),[55] and $Ca_3Y_{2-x}B_4O_{12}$:xEu^{3+} (88.57%).[14] Hence, these results indicate that GdYGd:Eu^{3+} phosphor is a great candidate for high color-purity LEDs.

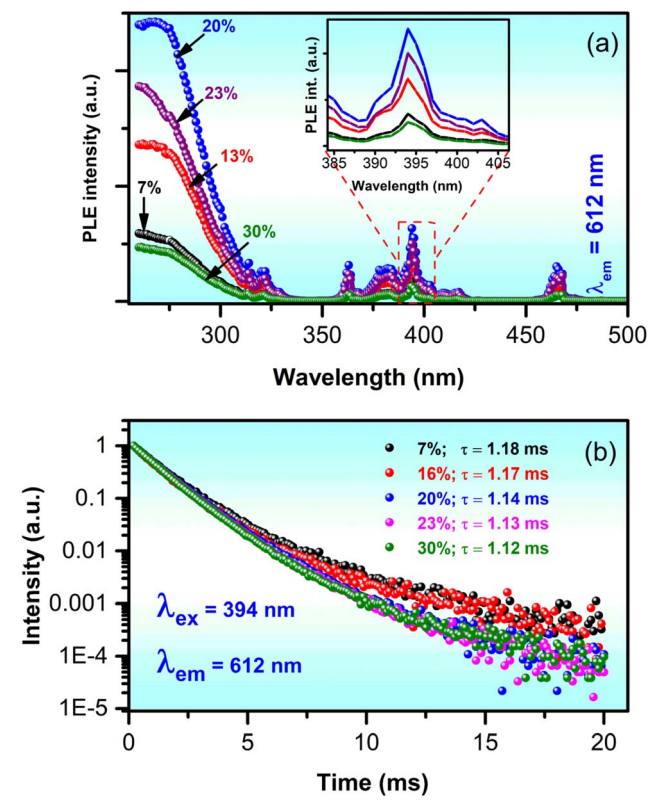

Fig. 9 (a) PLE spectra mentioned at 612 nm and (b) lifetime curves of GdYGd:x mol% Eu^{3+} (x = 7–30) phosphors.

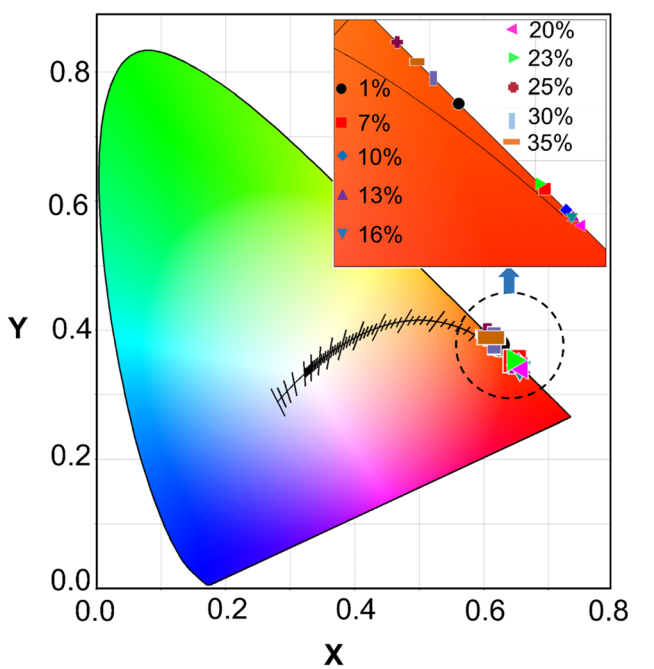

Fig. 10 CIE coordinates of GdYGd:Eu^{3+} phosphors doped with different concentrations in the range of 1–35 mol%.

Table 1 The calculated chromaticity coordinates and the color purity values of the GdYGd:x mol% Eu^{3+} (x = 1–35) phosphors

Eu^{3+} doping level (%)	Chromatic coordinates (x,y)	Color purity (%)
1	(0.6233,0.3762)	99.1
7	(0.6477,0.3520)	99.3
10	(0.6537,0.3460)	99.2
13	(0.6557,0.3440)	99.5
16	(0.6553,0.3444)	99.4
20	(0.6581,0.3416)	99.5
23	(0.6462,0.3535)	99.3
26	(0.6059,0.3936)	99.4
30	(0.6161,0.3834)	99.1
35	(0.6115,0.3880)	99.3

Fig. 11a illustrates the relationship between the optimized GdYGd:Eu^{3+} phosphor emission spectra and the measured temperature. It can be observed that all PL spectra in Fig. 11a present a similar shape; however, the PL intensity gradually decreases with the annealing temperature in the range of 25–200 °C, as illustrated in Fig. 11b. At 150 °C, the PL intensity remains 52.8% that of the initial PL intensity at room temperature. The activation energy (ΔE) of phosphors can be derived from the temperature-dependence spectra using the Arrhenius equation, as reported in our recent study.[8] The dependence of the $\left[\mathrm{Ln}\left[\left(\frac{I_0}{I}\right)-1\right]\right]$ on $1/kT$ is illustrated in the inset of Fig. 11b, showing a slope of −0.319 by linear fitting. Thus, the activation energy of the GdYGd:20 mol% Eu^{3+} phosphor is 0.319 eV. This obtained value is significantly better than some reported values for commercial phosphors, such as Y_2O_3:Eu^{3+} red phosphor (0.17–0.24 eV),[56,57] Sr_3YBO_3:0.9Eu^{3+} (0.137 eV),[3] and $Sr_9LiMg(PO_4)_7$:Eu^{3+} (0.160 eV).[58]

To demonstrate the application ability of the resultant phosphor, a prototype of a red-emitting LED was fabricated by coating the optimized GdYGd:20 mol% Eu^{3+} phosphor on the

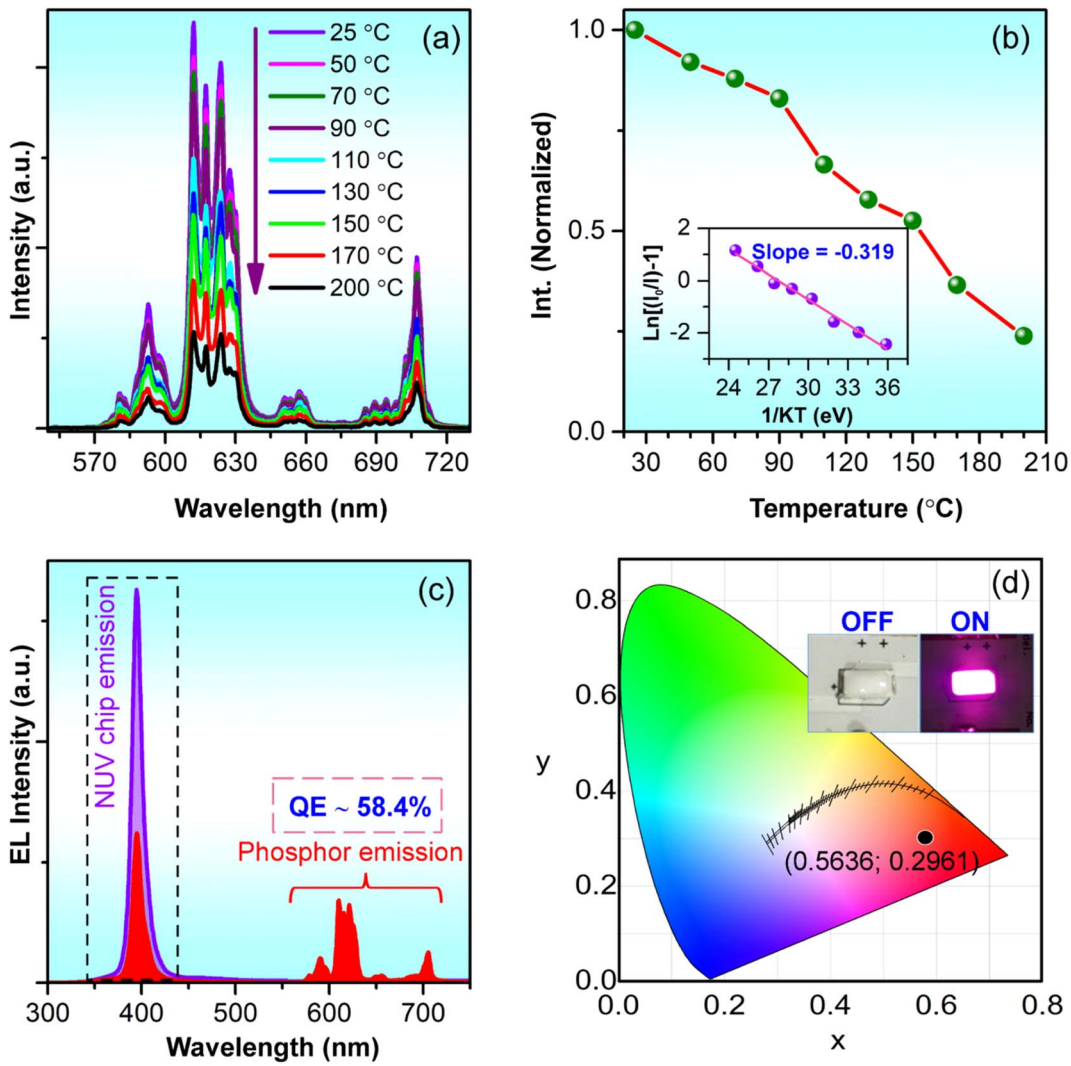

Fig. 11 (a) Temperature-dependent PL spectra of GdYGd:20 mol% Eu^{3+} phosphor and (b) the change in the normalized PL intensities based on the measured temperature. The inset in Fig. 10b shows the linear relationship between $\ln[(I_0/I) - 1]$ and $1/kT$. (c) EL spectra of the NUV chip (non-coated) and the GdYGd:20 mol% Eu^{3+}-coated NUV chip and (d) the CIE chromatic coordinates (x,y) of the red LED prototype. The inset in Fig. 10d shows a digital image of the red LED prototype at the OFF- and ON-mode states.

Table 2 A comparison of the QE values of recently reported red-emitting phosphors and the GdYGd:20 mol% Eu^{3+} phosphors

Phosphors	Excitation wavelength (nm)	Emission wavelength (nm)	QE (%)	Ref.
$AlPO_4$:3% Eu^{3+}	395	594	38.7	8
$K_4BaSi_3O_9$:0.05Eu^{3+}	395	617	27	62
$LiCaBO_3$:0.5% Eu^{3+}	393	611	40	63
CaB_4O_7:0.5% Eu^{3+}	393	611	48	63
$Na_3Sc_2(PO_4)_3$:0.35Eu^{3+}	394	621	49	64
KSGO:0.08Eu^{3+}	394	617	57.6	54
$Ca_8MgLu(PO_4)_7$:Eu^{3+}	394	612	69	65
$Ba_3Y_4O_9$:Eu^{3+}	396	614	46	66
YBO_3:0.05Eu^{3+}	394	591	44.59	67
Sr_2InTaO_6:Eu^{3+}	396	624	58.4	68
$La_2W_2O_9$:Eu^{3+}	395	618	77	69
$GdBO_3$:Eu^{3+}	391	591	14.3	18
$Gd(BO_2)_3$:Eu^{3+}	396	588	—	20
Y_3BO_6:Eu^{3+}	394	613	—	22
GdYGd:20% Eu^{3+}	**395**	**612**	**58.4**	**This study**

top surface of a 395 nm LED chip. Fig. 11c illustrates the EL spectra of the NUV LED chip (non-coated) and GdYGd:20 mol% Eu^{3+}-coated NUV LED. Additionally, a sharp emission peak at 395 nm from the NUV chip and red emissions in the 580–710 nm wavelength region is obvious in the EL spectrum of the GdYGd:Eu^{3+}-coated LED prototype. The quantum efficiency (QE) of GdYGd:20 mol% Eu^{3+} phosphor can be estimated using the following eqn (1):[59,60]

$$\mathrm{QE} = \frac{\int L_s}{\int E_R - \int E_s} \quad (1)$$

where L_S is the emission spectrum from the phosphor, and E_R and E_S correspond to the excitation spectra without and with the phosphor, respectively.[8,61]

Table 2 compares the QE values of some reported red-emitting phosphors and the optimized GdYGd:20 mol% Eu^{3+} phosphor in this study. The high QE value of 58.4% of the GdYGd:20 mol% Eu^{3+} phosphor indicates a potential application of this phosphor in NUV-pumped WLED. It is noteworthy that this value is much higher than the QE value of $GdBO_3$:Eu^{3+} phosphor (14.30%).[18] Fig. 11d illustrates the CIE chromatic coordinates ($x = 0.5636$,$y = 0.2961$) of the fabricated red LED. The inset presents the digital image of the red LED prototype in the OFF- and ON-mode states, demonstrating the strong red light emitted from this prototype.

4. Conclusion

A novel red-emitting Eu^{3+}-heavily doped $Gd(BO_2)_3$-Y_3BO_6-$GdBO_3$ phosphor well excited at 394 nm was successfully synthesized by applying a simple sol–gel method. Among the samples, the highest photoluminescence (PL) intensity is achieved when doped with a high concentration of 20 mol% Eu^{3+} and annealed at 1100 °C in an air atmosphere for 5 hours. The optimized phosphor shows excellent color purity of 99.5%, a high activation energy of 0.319 eV, and an impressive quantum efficiency of 58.4%. To demonstrate the practical application of this phosphor, a red LED prototype was successfully fabricated using the GdYGd:20 mol% Eu^{3+} phosphor, resulting in chromatic coordinates of ($x = 0.5636$,$y = 0.2961$). These results unequivocally demonstrate that the prepared $Gd(BO_2)_3$-Y_3BO_6-$GdBO_3$:20 mol% Eu^{3+} phosphor holds significant promise as an efficient candidate for phosphor materials in NUV-pumped WLED applications.

Conflicts of interest

There are no conflicts to declare.

Acknowledgements

This research is funded by the Vietnam National Foundation for Science and Technology Development (NAFOSTED) under grant number 103.03-2019.45.

References

1 T. Yaba, R. Wangkhem and N. S. Singh, *J. Alloys Compd.*, 2020, **843**, 156022.
2 G. Li, Y. Tian, Y. Zhao and J. Lin, *Chem. Soc. Rev.*, 2015, **44**, 8688–8713.
3 Z. Sun, Z. Zhu, J. Luo, Z. chao Wu, L. Zhou and X. Zhang, *Ceram. Int.*, 2019, **45**, 22517–22522.
4 Y. Jia, D. Xu, X. Yun, C. Wei, J. Zhou, J. Sun, S. Nay, P. O. F. Ce, Y. Jia, D. Xu, X. Yun, C. Wei, J. Zhou and J. Sun, *Optik*, 2020, **216**, 164895.
5 J. Li, Q. Liang, Y. Cao, J. Yan, J. Zhou, Y. Xu, L. Dolgov, Y. Meng, J. Shi and M. Wu, *ACS Appl. Mater. Interfaces*, 2018, **10**, 41479–41486.
6 A. Lakshmanan, R. S. Bhaskar, P. C. Thomas, R. S. Kumar, V. S. Kumar and M. T. Jose, *Mater. Lett.*, 2010, **64**, 1809–1812.
7 X. Huang, *Nat. Photonics*, 2014, **8**, 748–749.
8 M. T. Tran, N. Tu, N. V. Quang, N. D. Hung, L. T. H. H. Thu, D. Q. Trung and P. T. Huy, *J. Alloys Compd.*, 2020, **853**, 156941.
9 P. Pust, V. Weiler, C. Hecht, A. Tücks, A. S. Wochnik, A.-K. Henß, D. Wiechert, C. Scheu, P. J. Schmidt and W. Schnick, *Nat. Mater.*, 2014, **13**, 891–896.
10 Y. Zheng, H. Zhang, H. Zhang, Z. Xia, Y. Liu, M. S. Molokeev and B. Lei, *J. Mater. Chem. C*, 2018, **6**, 4217–4224.
11 L. T. Ha Thu, N. Tu, D. Duc Anh, D. Q. Trung, M. Trung Tran, T. T. Quynh Nhu, N. Thi Huyen, N. Van Quang, N. Duy Hung, D. Xuan Viet, N. D. Trung Kien and P. Thanh Huy, *ChemistrySelect*, 2021, **6**, 937–944.
12 H. Lin, D. Yang, G. Liu, T. Ma, B. Zhai, Q. An, J. Yu, X. Wang, X. Liu and E. Yue-Bun Pun, *J. Lumin.*, 2005, **113**, 121–128.
13 S. Neeraj, N. Kijima and A. K. Cheetham, *Chem. Phys. Lett.*, 2004, **387**, 2–6.
14 G. H. Li, N. Yang, J. Zhang, J. Y. Si, Z. L. Wang, G. M. Cai and X. J. Wang, *Inorg. Chem.*, 2020, **59**, 3894–3904.

15 P. Dang, G. Li, X. Yun, Q. Zhang, D. Liu, H. Lian, M. Shang and J. Lin, *Light: Sci. Appl.*, 2021, **10**, 1–13.
16 X. Zhang, L. Zhou and M. Gong, *Opt. Mater.*, 2013, **35**, 993–997.
17 A. Szczeszak, T. Grzyb, S. Lis and R. J. Wiglusz, *J. Chem. Soc., Dalton Trans.*, 2012, **41**, 5824–5831.
18 Z. Leng, N. Zhang, Y. Liu, L. Li and S. Gan, *Appl. Surf. Sci.*, 2015, **330**, 270–279.
19 Z. Leng, Y. Liu, N. Zhang, L. Li and S. Gan, *Colloids Surf., A*, 2015, **472**, 109–116.
20 F. Meng, X. Zhang, W. Li, T. Xie and H. J. Seo, *J. Phys. Chem. Solids*, 2012, **73**, 564–567.
21 D. Boyer, G. Bertrand-Chadeyron, R. Mahiou, A. Brioude and J. Mugnier, *Opt. Mater.*, 2003, **24**, 35–41.
22 Q. Zhu, Z. Fan, S. Wang, J. Xiahou and J. G. Li, *J. Am. Ceram. Soc.*, 2019, **102**, 7448–7461.
23 L. Sun, Y. Liu, B. Wang and S. Yang, *J. Alloys Compd.*, 2022, **899**, 163209.
24 N. Siraj, B. El-zahab, S. Hamdan, T. E. Karam, L. H. Haber, M. Li, O. Fakayode, S. Das, B. Valle, R. M. Strongin, G. Patonay, H. O. Sintim, G. A. Baker, A. Powe, M. Lowry, J. O. Karolin, C. D. Geddes and I. M. Warner, *Anal. Chem.*, 2016, **88**, 170–202.
25 N. T. Huyen, N. Tu, N. V. Quang, D. Quang Trung, M. T. Tran, N. V. Du, N. D. Hung, D. X. Viet, N. D. Trung Kien and P. T. Huy, *ACS Appl. Electron. Mater.*, 2021, **4**, 4322–4331.
26 N. Van Quang, N. Thi Huyen, N. Tu, D. Quang Trung, D. Duc Anh, M. T. Tran, N. D. Hung, D. X. Viet and P. T. Huy, *Dalton Trans.*, 2021, **50**, 12570–12582.
27 X. Zhang, F. Meng, W. Li, S. Il Kim, Y. M. Yu and H. J. Seo, *J. Alloys Compd.*, 2013, **578**, 72–76.
28 L. Yang, L. Zhou, Y. Huang and Z. Tang, *Mater. Lett.*, 2010, **64**, 2704–2706.
29 H. Forest and G. Ban, *J. Electrochem. Soc.*, 1971, **118**, 1999.
30 G. Jyothi and K. G. Gopchandran, *Dyes Pigm.*, 2018, **149**, 531–542.
31 J. Dalal, M. Dalal, S. Devi, R. Devi, A. Hooda, A. Khatkar, V. Taxak and S. Khatkar, *J. Lumin.*, 2019, **210**, 293–302.
32 Z. Wei, L. Sun, C. Liao, J. Yin, X. Jiang, C. Yan and S. Lü, *J. Phys. Chem. B*, 2002, **106**, 10610–10617.
33 Z. Wei, L. Sun, C. Liao, C. Yan and S. Huang, *Appl. Phys. Lett.*, 2002, **80**, 1447–1449.
34 L. Jia, Z. Shao, Q. Lü, Y. Tian and J. Han, *Ceram. Int.*, 2014, **40**, 739–743.
35 N. T. K. Lien, N. V. Thang, N. D. Hung, N. D. Cuong, N. D. T. Kien, C. X. Thang, P. H. Vuong, D. X. Viet, N. T. Khoi and P. T. Huy, *J. Electron. Mater.*, 2017, **46**, 3427–3432.
36 B. Fan, J. Liu, W. Zhou and L. Han, *Opt. Mater.*, 2019, **98**, 109499.
37 G. Z. Li, M. Yu, Z. L. Wang, J. Lin, R. S. Wang and J. Fang, *J. Nanosci. Nanotechnol.*, 2006, **6**, 1416–1422.
38 J. Li, Y. Wang and B. Liu, *J. Lumin.*, 2010, **130**, 981–985.
39 S. H. Shin, J. H. Kang, D. Y. Jeon, S. H. Choi, S. H. Lee, Y. C. You and D. S. Zang, *Solid State Commun.*, 2005, **135**, 30–33.
40 X. Cui, W. Zhuang, Z. Yu, T. Xia, X. Huang and H. Li, *J. Alloys Compd.*, 2008, **451**, 280–285.
41 H. Song, H. Q. Yu, G. Pan, X. Bai, B. Dong, X. T. Zhang and S. K. Hark, *Chem. Mater.*, 2008, **20**, 4762–4767.
42 Y. F. Liu, Z. P. Yang and Q. M. Yu, *J. Alloys Compd.*, 2011, **509**, L199–L202.
43 P. Li, Z. Yang, L. Pang, Z. Wang and Q. Guo, *J. Rare Earths*, 2008, **26**, 44–47.
44 C. Xiangzhong, Z. Weidong, Z. Xiying, X. Tian, L. Zhen, Y. Zhijian, Z. Chunlei and H. Xiaowei, *J. Rare Earths*, 2006, **24**, 149–152.
45 B. Van Hao, P. T. Huy, T. N. Khiem, N. T. Thanh Ngan, P. H. Duong, N. T. T. Ngan and P. H. Duong, *J. Phys.: Conf. Ser.*, 2009, **187**, 2009.
46 N. J. Shivaramu, E. Coetsee and H. C. Swart, *AIP Conf. Proc.*, 2018, **1953**, 1–5.
47 D. Kim, S. Yoon, C. Park, J. Park, B. Kim and B. Lee, *In SID Symposium Digest of Technical Papers*, 2001, vol. 32, pp. 742–745.
48 M. Seraiche, L. Guerbous, R. Mahiou and A. Potdevin, *Opt. Mater.*, 2020, **109**, 110339.
49 L. Shi, J. Li, Y. Han, W. Li and Z. Zhang, *J. Lumin.*, 2019, **208**, 201–207.
50 M. T. Tran, D. Q. Trung, N. Tu, D. D. Anh, L. T. H. Thu, N. Van Du, N. Van Quang, N. T. Huyen, N. D. T. Kien, D. X. Viet, N. D. Hung and P. T. Huy, *J. Alloys Compd.*, 2021, **884**, 161077.
51 A. Szczeszak, T. Grzyb, B. Barszcz, V. Nagirnyi, A. Kotlov and S. Lis, *Inorg. Chem.*, 2013, **52**, 4934–4940.
52 W. Pan, P. Wang, Y. Xu and R. Liu, *Thin Solid Films*, 2015, **578**, 69–75.
53 N. Van Quang, N. Thi Huyen, D. Quang Trung, D. Duc Anh, M. T. Tran, H. D. Nguyen, D. X. Viet and P. T. Huy, *Dalton Trans.*, 2021, **50**, 12570–12582.
54 Q. Zhang, X. Wang and Y. Wang, *Inorg. Chem. Front.*, 2020, **7**, 1034–1045.
55 X. Huang, H. Guo and B. Li, *J. Alloys Compd.*, 2017, **720**, 29–38.
56 M. Fhoula and M. Dammak, *J. Lumin.*, 2020, **223**, 117193.
57 S. Som, S. Das, S. Dutta, H. G. Visser, M. K. Pandey, P. Kumar, R. K. Dubey and S. K. Sharma, *RSC Adv.*, 2015, **5**, 70887–70898.
58 J. Luo, Z. Sun, Z. Zhu, X. Zhang, Z. Wu and F. Mo, *Ceram. Int.*, 2020, **46**, 11994–12000.
59 Y. Han, L. Shi, H. Liu and Z. Zhang, *Optik*, 2019, **195**, 162014.
60 D. Q. Trung, N. V. Quang, M. T. Tran, N. V. Du, N. Tu, N. D. Hung, D. X. Viet, D. D. Anh and P. T. Huy, *Dalton Trans.*, 2021, **50**, 9037–9050.
61 D. Q. Trung, N. Tu, N. V. Quang, M. T. Tran, N. V. Du, P. T. Huy, N. Tu, N. V. Quang, M. T. Tran, N. V. Du and P. T. Huy, *J. Alloys Compd.*, 2020, **845**, 156326.
62 D. Stefańska, M. Stefański and P. J. Dereń, *Opt. Mater.*, 2014, **37**, 410–413.
63 I. I. Kindrat and B. V. Padlyak, *Opt. Mater.*, 2018, **77**, 93–103.
64 H. Guo, X. Huang and Y. Zeng, *J. Alloys Compd.*, 2018, **741**, 300–306.

65 F. Xie, Z. Dong, D. Wen, J. Yan, J. Shi, J. Shi and M. Wu, *Ceram. Int.*, 2015, **41**, 9610–9614.
66 J. Liang, L. Sun, G. Annadurai, B. Devakumar, S. Wang, Q. Sun, J. Qiao, H. Guo, B. Li and X. Huang, *RSC Adv.*, 2018, **8**, 32111–32118.
67 B. Liu, X. Xiao, J. Yu, D. Mao and G. Lu, *RSC Adv.*, 2016, **6**, 69442–69453.
68 J. Zhao, H. Gao, H. Xu, Z. Zhao, H. Bu, X. Cao, L. He, Z. Yang and J. Sun, *RSC Adv.*, 2021, **11**, 8282–8289.
69 Q. Cheng, F. Ren, Q. Lin, H. Tong and X. Miao, *J. Alloys Compd.*, 2019, **772**, 905–911.